SCIENCE CHINA
Earth Sciences

• RESEARCH PAPER •

December 2014 Vol.57 No.12: 3062–3072
doi: 10.1007/s11430-014-4984-3

Joint statistical-dynamical approach to decadal prediction of East Asian surface air temperature

LUO FeiFei[1,2] & LI ShuangLin[1,2*]

[1] *Nansen-Zhu International Research Centre, Institute of Atmospheric Physics, Chinese Academy of Sciences, Beijing 100029, China;*
[2] *Climate Change Research Center and Key Laboratory of Regional Climate Environment for East Asia, Chinese Academy of Sciences, Beijing 100029, China*

Received February 27, 2014; accepted August 8, 2014; published online October 29, 2014

A joint statistical-dynamical method addressing both the internal decadal variability and effect of anthropogenic forcing was developed to predict the decadal components of East Asian surface air temperature (EATs) for three decades (2010–2040). As previous studies have revealed that the internal variability of EATs (EATs_int) is influenced mainly by the ocean, we first analyzed the lead-lag connections between EATs_int and three sea surface temperature (SST) multidecadal modes using instrumental records from 1901 to 1999. Based on the lead-lag connections, a multiple linear regression was constructed with the three SST modes as predictors. The hindcast for the years from 2000 to 2005 indicated the regression model had high skill in simulating the observational EATs_int. Therefore, the prediction for EATs_int (Re_EATs_int) was obtained by the regression model based on quasi-periods of the decadal oceanic modes. External forcing from greenhouse gases is likely associated with global warming. Using monthly global land surface air temperature from historical and projection simulations under the Representative Concentration Pathway (RCP) 4.5 scenario of 19 Coupled General Circulation Models participating in the fifth phase of the Coupled Model Intercomparison Project (CMIP5), we predicted the curve of EATs (EATs_trend) relative to 1970–1999 by a second-order fit. EATs_int and EATs_trend were combined to form the reconstructed EATs (Re_EATs). It was expected that a fluctuating evolution of Re_EATs would decrease slightly from 2015 to 2030 and increase gradually thereafter. Compared with the decadal prediction in CMIP5 models, Re_EATs was qualitatively in agreement with the predictions of most of the models and the multi-model ensemble mean, indicating that the joint statistical-dynamical approach for EAT is rational.

East Asia, surface air temperature, decadal prediction, internal decadal variability, anthropogenic forcing

Citation: Luo F F, Li S L. 2014. Joint statistical-dynamical approach to decadal prediction of East Asian surface air temperature. Science China: Earth Sciences, 57: 3062−3072, doi: 10.1007/s11430-014-4984-3

Decadal climate prediction focuses on predicting time-evolving regional climate conditions over the next 10–30 years, which has to take into account the initialization of the climate system (ocean conditions), the interaction of the natural internal variability, and the impact of external forcing. Traditionally, it was difficult to achieve decadal prediction due to a lack of observational datasets and efficient research methods, as well as a limited understanding of the climate on the multidecadal timescale. In recent years, satellite datasets have become more prevalent, and the technologies of assimilation and climate system models have improved rapidly. As a result, it is now possible to make decadal predictions with better accuracy. Because understanding the climate on the decadal timescale is a priority if human populations are to adapt to climate change, decadal prediction—currently in its infancy—has emerged as a hot topic in the field of climate research (Meehl et al., 2009; Hurrell et al., 2010; Murphy et al., 2010). It is one of two distinct focuses in the fifth phase of the Coupled Model

*Corresponding author (email: shuanglin.li@mail.iap.ac.cn)

Intercomparison Project (CMIP5) under the Intergovernmental Panel on Climate Change (IPCC) Special Reports (Taylor et al., 2012).

Methods of climate prediction mainly fall into one of three categories: the dynamical approach, the statistical approach, and the joint statistical-dynamical approach. Of these, the dynamical approach is applied most frequently worldwide. There are two types of dynamical approach: the "one-tiered" approach and the "two-tiered" approach. The one-tiered approach obtains predictions by offering initial fields and external forcing to a coupled atmosphere-ocean general circulation model (AOGCM) and then integrating them directly (Smith et al., 2007; Keenlyside et al., 2008; Pohlmann et al., 2009; Mochizuki et al., 2010). The two-tiered approach involves two steps: First, the predicted lower-boundary forcing (sea surface temperature, SST) is obtained by coupled general circulation models (CGCMs) or statistics (Hoerling et al., 2011). Second, the climate is predicted with an atmospheric general circulation model (AGCM) based on the predicted lower-boundary forcing. The one-tiered approach has been commonly applied in China. For example, decadal hindcast and forecast experiments were performed by the FGOALS_gl and FGOALS_g2 CGCMs developed by the State Key Laboratory of Numerical Modeling for Atmospheric Sciences and Geophysical Fluid Dynamics, the Institute of Atmospheric Physics, Chinese Academy of Sciences (Wu and Zhou, 2012; Wang et al., 2012). Gao et al. (2012) evaluated the prediction capability of the Beijing Climate Center Climate System Model (BCC-CSM1.1) with respect to regional and global surface temperatures on the decadal timescale. Chen and Jiang (2012) pointed out that there was a cold bias in the temperature field in multi-decadal hindcast results of four CGCMs that were involved in the ENSEMBLES project, and that the level of uncertainty was quite large. This great uncertainty in the dynamic prediction resulted from a shortage of sub-surface oceanic observational data, a defect in the technology of assimilation, and climate drift induced by the imperfection of the models themselves.

In addition to the one-tiered approach, some scientists have also exploited statistical approaches for decadal prediction. Qian et al. (2010) predicted that a cool floor of global-mean surface air temperature (GSAT) would appear in the 2030s based on the sum of principal harmonics and the linear trend of GAST. Fu et al. (2011) utilized empirical mode decomposition to project GSAT for the next 40 years, and suggested that global warming during 2011–2050 could be much weaker than the projection reported in IPCC AR4. These studies indicate that statistical approaches are feasible; however, they also have their limitations. For example, Hawkins et al. (2011) evaluated the potential of statistical decadal predictions of SSTs in a perfect-model analysis, and pointed out that the predictions depended on the predicted region, time, and modeled data used.

Given that the joint statistical-dynamical approach combines the two sets of advantages of the dynamical and statistical approaches, it has been widely used and successfully in short-term climate prediction. Luo et al. (2012) developed a simple approach that considers both the quasi-periodicities of internal decadal oceanic models and the effect of anthropogenic forcing to predict the decadal components of global SSTs. Abnormalities of observational climate are formed by the natural internal variability and effects of external forcing. The natural internal variability includes timescale-type variabilities such as interannual variability (e.g., ENSO, AO/AAO), multi-decadal variability (e.g., AMO, PDO), and centennial variability. Because decadal internal variability is influenced mainly by decadal oceanic modes, the quasi-periods of oceanic modes make it possible to predict the temporal evolution of decadal variability using the statistical approach. The external forcing consists of natural forcing (e.g., volcanos, solar radiation) and anthropogenic forcing. It is hard to predict volcanic eruptions based on current technology. The evolution of solar radiation can be predicted due to its quasi-11-year cycle. The effects of human activity on the climate mainly manifest through emissions of greenhouse gases and aerosols into the atmosphere. CMIP3 OGCMs projected climate changes in the twenty-first century under the A1, A1B, B1, and B2 emissions scenarios. The datasets help us to understand the impacts of greenhouse gases on future climate. Relative to CMIP3, the four CMIP5 Representative Concentration Pathway (RCP) scenario runs (RCP2.6, RCP4.5, RCP6 and RCP8.5), which provided a range of simulated climate change, can be used to explore the impacts of anthropogenic activity. As mentioned above, it may become possible to achieve decadal prediction of East Asian surface air temperature (EATs) using joint statistical-dynamical approaches.

There has been little research published on the decadal prediction of EATs. With this in mind, the present study not only provides a new method for decadal prediction, but also affords a sample of the evolution of EATs over the next 10–30 years. First, we calculated the lead-lag connections of the internal variability of EATs (EATs_int) and multi-decadal SST modes in instrumental records. Based on the connections, a multiple linear regression model, with the multi-decadal SST modes as predictors, was established to predict EATs_int. In the next step, the change of EATs caused by anthropogenic forcing was obtained using a second-order fit. Outputs of the historical and projected experiments in CMIP5 were used, spanning the period from 1901 to 2040. The results of the two parts were then combined to reconstruct and predict the decadal components of EATs.

1 Data and methods

1.1 Data

The monthly global land surface air temperature (T_s) for 1901–2009, on a 0.5°×0.5° grid, was obtained from the

Climate Research Unit (CRU) TS 3.1 dataset (Mitchell and Jones, 2005). Two sets of observational SST were used, spanning the years 1870–2010. One was the Met Office Hadley Centre's monthly SST records (HadISST) (Rayner et al., 2003), gridded to 1.0° latitude by 1.0° longitude. The other was the Kaplan Extended monthly SST (Kaplan et al., 1998), on a 5°×5° grid.

The modeled monthly global T_s was used based on the three types of experiments in CMIP5: (1) a future projection simulation forced by a midrange mitigation emissions scenario (RCP4.5) in 19 models, covering 2006–2040; (2) a 30-year decadal prediction initialized in 2005 in eight models, ranging from 2006–2035; and (3) outputs from historical experiments from the (1) and (2) CGCMs, spanning 1901–2005. Key model details are listed in Tables 1 and 2. Outputs were downloaded from the project for model diagnostics and intercomparisons (PCMDI) CMIP5 website (http://pcmdi9.llnl.gov/esgf-web-fe/).

1.2 Methods

EATs is impacted by both natural internal variability and external forcing. The internal decadal variability is modulated primarily by oceanic thermal conditions. We evaluated the rationality of three SST modes (the Atlantic Multidecadal Oscillation, the Inter-decadal Pacific Oscillation, and the Indian Ocean Basin-wide Decadal Pattern) as factors to predict EATs_int. The correlations of these modes with EATs_int and the proportions of explained variance were calculated.

The proportion of explained variance (S_p) is defined as $S_p = S_{\hat{y}} / S_y$, where S_y is the SST (EATs_int) variance and $S_{\hat{y}}$ is the variance of $\hat{y}$. $\hat{y}$ is the SST (EATs_int) associated with the time series of SST modes (X_k), which is obtained by the linear fitting equation $\hat{y}(t) = b_1 X_k$. In this equation, b_1 is the regression coefficient calculated by the

Table 1 List of historical simulations and projected simulations under the RCP4.5 scenario with 19 CMIP5 models

Modeling groups	Model ID	Resolution (Lat × Lon)
CSIRO-BOM, Australia	ACCESS1.0	1.875°×1.25°
	ACCESS1.3	
Beijing Climate Center (BCC), China	BCC-CSM1.1	2.8125°×2.8125°
	BCC-CSM1.1 (m)	1.125°×1.125°
National Center for Atmospheric Research (NCAR), USA	CCSM4	1.25°×0.9375°
	CESM1-BGC	
	CESM1-CAM5	
CSIRO-QCCCE, Australia	CSIRO-Mk3.6.0	1.875°×1.875°
The First Institute of Oceanography, China	FIO-ESM	2.8125°×2.8125°
NASA Goddard Institute for Space Studies, USA	GISS-E2-H	2.5°×2°
	GISS-E2-R	
Met Office Hadley Centre, UK	HadGEM2-CC	1.875°×1.24°
Institute for Numerical Mathematics, Russia	INM-CM4	2°×1.5°
Institute Pierre-Simon Laplace (IPSL), France	IPSL-CM5A-LR	3.75°×1.875°
	IPSL-CM5A-MR	2.5°×1.258°
	IPSL-CM5B-LR	3.75°×1.875°
Max Planck Institute for Meteorology (MPI-M), Germany	MPI-ESM-LR	1.875°×1.875°
Meteorological Research Institute, Japan	MRI-CGCM3	1.125°×1.125°
Norwegian Climate Center, Norway	NorESM1-ME	2.5°×1.875°

Table 2 List of historical simulations and decadal predictions with eight CMIP5 models

Modeling groups	Model ID	Resolution (Lat × Lon)
Beijing Climate Center (BCC), China	BCC-CSM1.1	2.8125°×2.8125°
Canadian Center for Climate Modelling and Analysis, Canada	CanCM4	2.8125°×2.8125°
Euro-Mediterranean Center on Climate Change, Italy	CMCC-CM	0.75°×0.75°
Météo-France/Centre National de Recherches Météorologiques, France	CNRM-CM5	1.40625°×1.40625°
LASG, Institute of Atmospheric Physics, China	FGOALS-g2	3°×2.8125°
Institute Pierre-Simon Laplace (IPSL), France	IPSL-CM5A-LR	3.75°×1.875°
Max Planck Institute for Meteorology (MPI-M), Germany	MPI-ESM-LR	1.875°×1.875°
Meteorological Research Institute, Japan	MRI-CGCM3	1.125°×1.125°

least-squares estimation method. Based on the periodicities of X_k, X_k can be predicted by harmonic analysis. EATs_int is then predicted via the multiple linear regression model with predictors of the three modes, based on the respective lead-lag correlations between the SST modes and EATs_int. Since the industrial revolution, the impacts of external forcing are likely to be associated with global warming induced by greenhouse gases, which can be established by determining the trend of EATs (EATs_trend) via the second-order fit. It should be pointed out that EATs_trend contains both the centennial-scale variability and the signal of global warming. First, we respectively calculated the modeled EATs_trend using data from the historical and projection runs under the RCP4.5 scenario. The multi-model ensemble (MME) mean was then seen as the change of EATs induced by anthropogenic forcing. Finally, EATs_int and EATs_trend were combined to reconstruct the EATs, before performing the hindcast and prediction.

For the internal variability, the uncertainty of the oceanic modes or EATs_int was estimated via the ±1 standard deviation range itself. For the external forcing, the model spread was used to evaluate the uncertainty of EATs_trend. The larger the value of the model spread, the wider the disparity among the climate models, and hence a greater level of uncertainty. Given that this paper focuses on the prediction of the decadal components of EATs, all datasets were filtered with a nine-point running-mean filter to obtain low-frequency components. The indices of these oceanic modes and EATs_int were detrended to reduce the possible anthropogenic impacts, based on the assumption that the impact of anthropogenic forcing on the climate is linear. Here, the climatic period is from 1970 to 1999.

2 Predicted model for EATs_int with the oceanic modes as the predictor

2.1 Oceanic modes

The Atlantic Multidecadal Oscillation (AMO) is a leading fluctuation pattern of SST in the North Atlantic region, which has been linked to the Meridional Overturning Circulation (MOC) in many models (Delworth and Mann, 2000; Enfield et al., 2001; Sutton and Hodson, 2005, 2007; Knight et al., 2005). The AMO has a period of 65 years and an amplitude of 0.4°C in instrumental records (Delworth and Mann, 2000; Enfield et al., 2001; Sutton and Hodson, 2005). Following earlier AMO definitions (Enfield et al., 2001; Wang et al., 2009), the AMO index was defined as the annual averaged low-frequency SST anomaly (SSTA) in the North Atlantic basin (0°–60°N, 75°–7.5°W). The temporal evolution of AMO index (dashed line in Figure 1(a)) is characterized by two cold phases from the early-1900s to

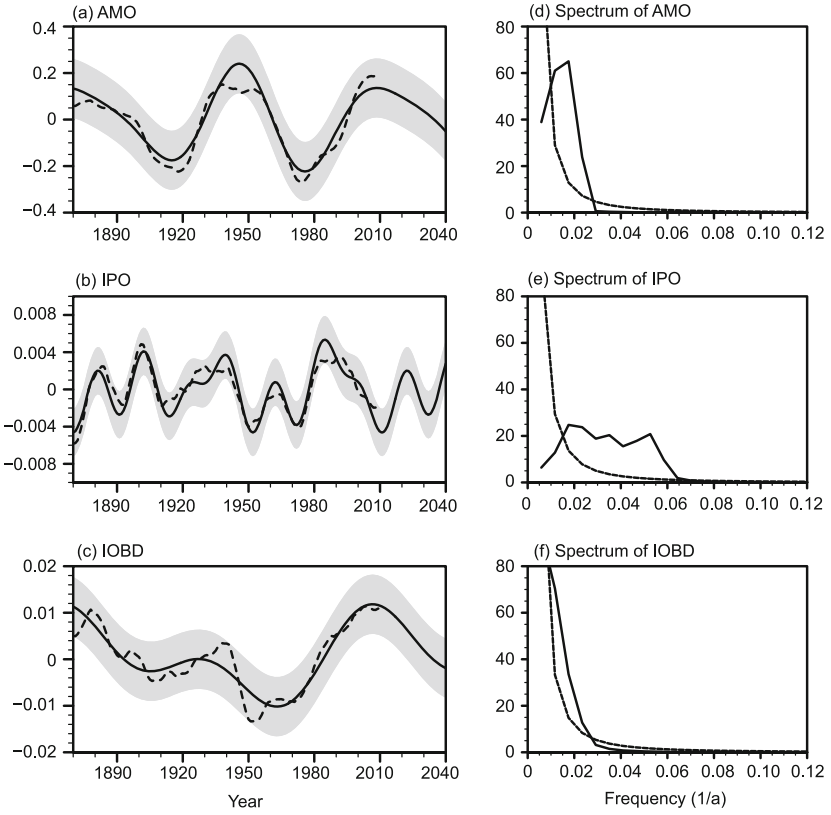

Figure 1 Annual averaged temporal evolution and power spectrum of oceanic modes. (a)–(c) The original AMO, IPO, and IOBD indices from 1870 to 2010 (dashed lines); principal component (PC) of the indices from 1870 to 2040 (solid lines); ±1 standard deviation range (gray shading). Unit: °C. (d)–(f) Power spectrum of the PCs of indices (solid lines); significance level (α = 0.05) of a standard red noise spectrum (dashed lines).

the late-1920s and from the mid-1960s to the 1990s, and two warm phases from the 1930s to the 1960s and from the mid-1990s until now. These are in agreement with previous studies (Delworth and Mann, 2000; Enfield et al., 2001; Sutton and Hodson, 2005, 2007; Knight et al., 2005; Wang et al., 2009). Figure 2(a) shows that the AMO explains approximately 50% of the internal decadal variance of SSTs over the North Atlantic. In particular, the proportions of variance are greater than 70% over the tropical and eastern North Atlantic. Besides, the proportion is approximately 50% in the western tropical Pacific.

The Inter-decadal Pacific Oscillation (IPO) is the decadal climate variability in the leading Pacific SST pattern. During the positive phase, the IPO is marked mainly by cool anomalies over the mid-high latitudes of the South and North Pacific, while it is warm along the west coast of the United States and the tropical Pacific (Power et al., 1999; Folland et al., 1999). The situation is opposite in the negative phase. The IPO index is defined as the time series of the first empirical orthogonal function (EOF) of SSTAs in the Pacific basin (60°S–60°N, 120°E–80°W) (Power et al., 1999; Folland et al., 1999). The first mode accounts for 43% of Pacific SSTs. The IPO (dashed line in Figure 1(b)) experiences one cold period from the mid-1940s to the mid-1970s, and two warm periods from the 1920s to 1940s and from the 1970s to 1990s. The warm phase of the IPO shifts to a cold phase at the beginning of the 21st century. This is consistent with previous results (Folland et al., 1999). The IPO is the most important in the tropical mid-eastern Pacific, explaining 60% of the variance. In the mid-high latitudes of the Pacific, the proportion is approximately 50% (Figure 2(b)).

The Indian Ocean Basin-wide Decadal (IOBD) pattern is characterized by a uniform basin-wide warming or cooling in the Indian Ocean on the decadal timescale (Allan et al., 1995; Li et al., 2012). The IOBD pattern is defined as the leading EOF of SSTAs over the Indian Ocean (20°S–25°N, 35°–120°E), which explains 70% of the total variance. From the dashed line in Figure 1(c), it can be seen that the IOBD pattern has a warm period from the 1870s to the late 1880s, and subsequently moves into a cold phase with a weak amplitude in the 1890s until the 1950s. The IOBD pattern remains in a cold phase from the 1950s to 1980s, and thereafter shifts to a warm phase. Figure 2(c) shows that the IOBD pattern is more important over the tropical Indian Ocean and western Pacific (eastern Philippine Sea) and explains approximately 60% of the variance.

Accordingly, the AMO, IPO, and IOBD pattern represent the leading mode of the internal decadal variance of SST in the North Atlantic, Pacific, and Indian Ocean, respectively. The sum of the proportions of variance of the three modes is greater than 90% over most of the North Atlantic, tropical mid-eastern Pacific, Indian Ocean, and parts of the western Pacific (Figure 2(d)).

2.2 Connections of the oceanic modes with EATs_int

An index of EATs_int was defined as the T_s anomalous mean over the domain (22.5°–45°N, 100°–125°E), as was done in previous studies (Wang et al., 2009; Li and Luo, 2013). There are two cold periods and two warm periods during the past 100 years (see Figure 1(a) in Li and Luo (2013)). The two cold periods are from the early 1900s to 1920s and from the 1950s to the early 1990s, whereas the warm periods are from the 1920s to the late 1940s and from the mid-1990s to now. EATs_int has an amplitude of 0.6°C

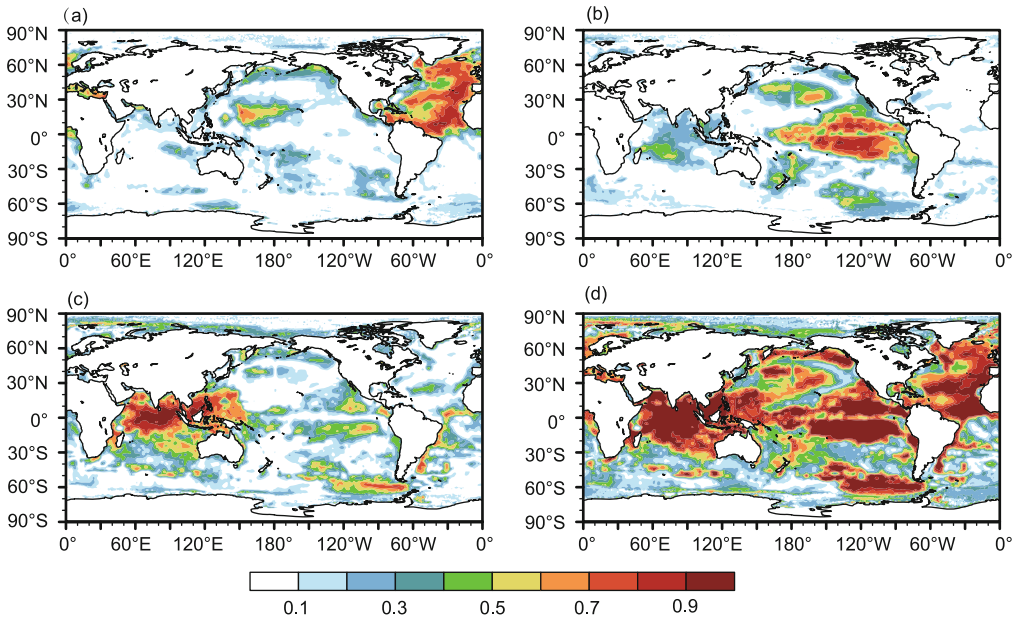

Figure 2 Proportion of explained variance for (a) AMO, (b) IPO, (c) IOBD pattern and (d) AMO+IPO+IOBD relative to the decadal internal SST variability.

and a significant period of 60–70 years.

Figure 3 shows the lead-lag correlation coefficients of the AMO, IPO, and IOBD pattern with EATs_int. When EATs_int leads the AMO by 6 years, a positive correlation reaches a maximum (correlation coefficient of 0.79). This is contrary to the connection of the IPO/IOBD pattern with EATs_int. When the IPO (IOBD pattern) leads EATs_int by 10 (5) years, a positive correlation reaches a maximum, with correlation coefficients of 0.56 (0.74). As we know, the response of the atmosphere to SST is a rapid process. Hence, the simultaneous correlation between the AMO and EATs should be the strongest. However, this finding that EATs_int leads the AMO challenges the traditional view. Li and Luo (2013) proposed two hypotheses to explain the connection between the AMO and EATs: (1) external forcing disturbs the intrinsic connection of the climate system; and (2) a connection exists via some processes of the climate system itself, such as the "the atmospheric bridge", "oceanic bridge" or atmosphere-ocean interaction. Unfortunately, due to a lack of observational datasets, it is difficult to validate the connection and investigate the physical mechanism at present. When the correlation between the AMO and EATs is strongest, the AMO explains approximately 40% of EATs_int in the Midwest (Figure 4(a)), which is in agreement with a previous study (Li and Bates, 2007). The IOBD pattern accounts for more than 30% above 30°N (Figure 4(b)), whereas the IPO is less than 10% in most of East Asia (Figure 4(c)). The total of proportions is greater than 60% in the Midwest and north, and nearly 30% in the region south of 30°N (Figure 4(d)).

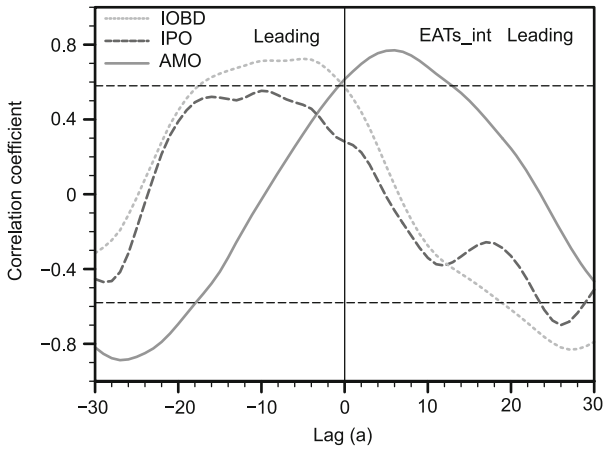

Figure 3 Lead-lag correlations: AMO-EATs_int (solid line); IPO-EATs_int (dashed line); IOBD-EATs_int (dotted line).

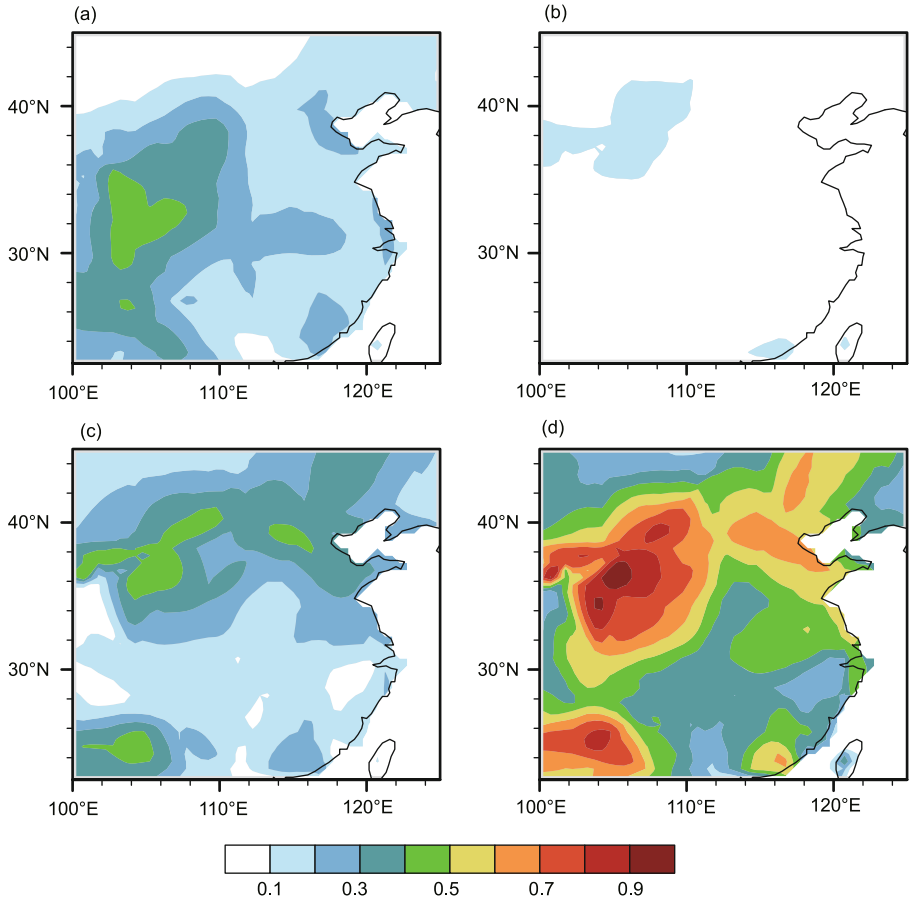

Figure 4 Proportion of explained variance for (a) AMO, (b) IPO, (c) IOBD pattern, and (d) AMO+IPO+IOBD relative to EATs_int when the correlations of the oceanic modes with EATs_int are strongest.

Similar lead-lag correlations were calculated among the AMO, IPO, and the IOBD pattern. The simultaneous correlation between the AMO and IPO is much less significant (correlation coefficient of less than 0.1). When the AMO leads the IPO by 17 years, their correlation is the strongest negative (−0.66), and when the AMO lags the IPO by 20 years their correlation is the strongest positive. A similar result was obtained by d'Orgeville and Peltier (2007). There is also no significant simultaneous connection between the AMO and IOBD pattern, with a coefficient of 0.33. When the AMO lead period is 19 years, the negative correlation reaches a maximum (−0.66), but when the AMO lags the IOBD pattern the correlation is less significant. Either the simultaneous or the lead-lag correlations between the IPO and IOBD pattern are much less significant.

2.3 Predicted models for EATs_int and validation

On the basis of the lead-lag correlations of the AMO, IPO, and IOBD pattern with EATs_int, we constructed eq. (1) with a multiple linear regression,

$$\begin{aligned}\mathrm{EATs\_int}(t) = b_0 + b_1 X_{\mathrm{AMO}}(t+6) + b_2 X_{\mathrm{IPO}}(t-10) \\ + b_3 X_{\mathrm{IOBD}}(t-5),\end{aligned} \quad (1)$$

where t is time, b_0, b_1, b_2, b_3 are regression coefficients; EATs_int is the mean of the Ts anomaly over the domain (22.5°–45°N, 100°–125°E); and X_{AMO}, X_{IPO}, X_{IOBD} are the time series of principal components (PCs) by harmonic analyses based on the original indices of the AMO, IPO, and IOBD pattern (black solid lines in Figure 1(a)–(c)). The purpose of harmonic analysis is to obtain the PCs of the original indices and predict the time evolution of these indices in future. Due to the great differences among the periods of the three oceanic modes, the instrumental data have different numbers of full cycles for different modes. Therefore, different harmonic components were selected for different modes. One harmonic was used to reconstruct the X_{AMO}, which captures 83% of the AMO index; four harmonics were used to reconstruct the X_{IPO}, which captures 70%; and two harmonics were used to reconstruct the X_{IOBD}, which captures 81%. Based on the periodicities of harmonic series, the time evolutions of indices can be predicted. In Figure 1(a) and (c), both of the predicting AMO and IOBD indices begin to fall at 2010 and shift to a negative phase around 2040. The predicting IPO index (Figure 1(b)) is characterized by one and a half fluctuations from 2010 to 2040. The index has a positive phase during 2015–2025 and a negative phase during 2025–2035. After 2035, it changes into a positive phase.

As verification, the power spectrums of X_{AMO}, X_{IPO}, X_{IOBD} were used to evaluate whether or not these PCs can represent the periods of the oceanic modes. From Figures 1(d)–(f), the three periods are 50 years, 20–50 years, and 70 years, respectively. Hence, X_{AMO}, X_{IPO}, X_{IOBD} reflect the primary periods of the original indices. The regression model of EATs_int (eq. (1)) is established using time series of EATs_int and X_{AMO}, X_{IPO}, X_{IOBD} from 1905 to 1999, where X_{AMO}, X_{IPO}, X_{IOBD} are the factors. The regression coefficients (b_0=−0.04, b_1=0.13, b_2=−0.04, b_3=0.18) were then obtained by the least-squares method. These regression coefficients were substituted into eq. (1) to obtain the reconstructed EATs_int, referred to as Re_EATs_int. The hindcasted Re_EATs_int from 2000 to 2005 was compared to the observation, with the values from 2006 to 2040 as a prediction. It can be seen that Re_EATs_int captures the main features of EATs_int to a certain extent (red dashed line in Figure 5), as indicated by the high correlation coefficient of 0.7. For example, the two warm phases from the 1920s to 1950s and from the mid-1990s to now in EATs_int exist in Re_EATs_int, as do the two cold phases. However, Re_EATs_int cannot simulate the period of 20 years in EATs_int. One reason for this could be that the impact of the IPO with the period of 20 years on EATs_int is weaker than the impacts from the AMO or IOBD pattern. Another reason could be that some predictors with the period of 20–30 years were not considered.

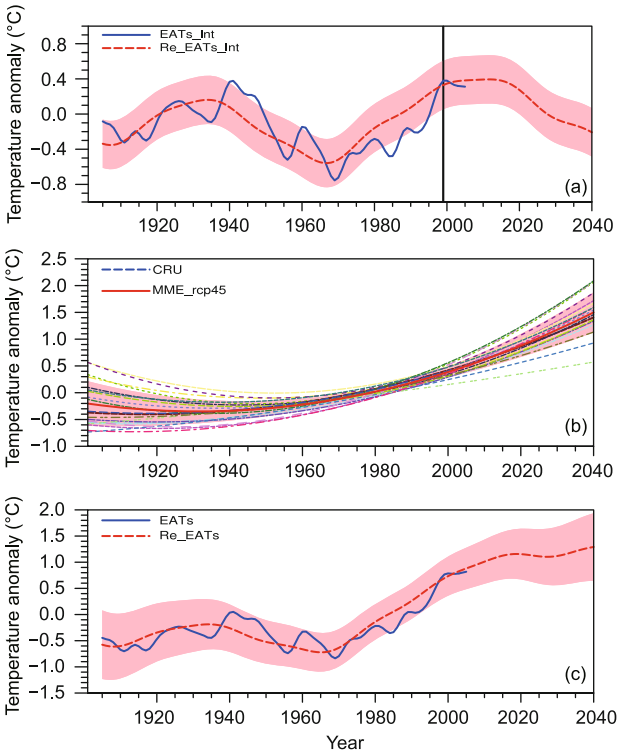

Figure 5 Annual averaged temporal evolution of East Asian surface temperature indices. (a) EATs_int from 1901 to 2009 (blue solid line) and Re_EATs_int from 1901 to 2040 (red dashed line): reconstructed period (1905–1999); hindcast period (2000–2005); predicted period (2006–2040). The light red shading indicates the ±1 standard deviation range of Re_EATs_int. (b) EATs trend by a second-order fit in different models (colored thin lines), multi-model ensemble mean (red solid line), and observations (blue dashed line), relative to 1970–1999. The light red shading indicates the model spread. (c) Same as EATs_int, but for EATs. Unit: °C.

In Figure 5(a), for the hindcast from 2000 to 2005, the mean of Re_EATs_int is 0.37°C, which is quite close to the observational mean of 0.34°C. This indicates the predicted model has a certain degree of prediction skill. Re_EATs_int remains stable throughout 2006–2015, and thereafter begins to fall. Up until 2025, Re_EATs_int shifts into a negative phase. This is in agreement with the prediction of Qian et al. (2010) for GSAT, which they showed will begin a cold period in the 2030s. Quantitatively, given the ±1 standard deviation ranges of the AMO, IPO, and IOBD pattern (±0.35°C, ±0.008°C, and ±0.02°C) (gray shading in Figure 1(a)–(c)), we could easily estimate Re_EATs_int to be −0.2±0.27°C in 2040 upon the predicted model.

3 Predicted trend of EATs based on the impact of greenhouse gases

The main effect of anthropogenic forcing is global warming induced by emissions of greenhouse gases after the Industrial Revolution. The long-term trend of observational EATs with a warming rate of 0.87°C/100 a increases by about 1°C from 1901 to 2010 (thick blue dashed line in Figure 5(b)). The warming rate is roughly equivalent to the rate of 0.81°C/100 a (Tang and Ren, 2005). The colored thin lines in Figure 5(b) display the trends of EATs according to the CMIP5 models. The correlation coefficients between the modeled and observed trends are summarized in Table 3. Apart from CSIRO-Mk3.6.0 and HadGEM2-CC, the other models perform well in simulating the upward trend of EATs, exhibiting high correlation coefficients (>0.7). The range of root-mean-square error (RMSE) is from 0.001°C to 0.04°C (Table 3). CCSM4, with an RMSE of 0.001°C exhibits the highest skill in simulating the observed long-term trend. CCSM4 predicts that EATs will increase to 1.4°C by 2040. Besides, the RMSEs of CSIRO-Mk3.6.0 and HadGEM2-CC are the highest among the models.

The long-term trend of the MME mean (MME_rcp45) bears a strong resemblance to the observation (thick red solid line in Figure 5(b)), showing a linear trend of 0.74°C/100 a during 1901–2009, a high correlation coefficient of 0.98, and a small RMSE of 0.005°C. The mean MME_rcp45 of −0.01°C during 1901–2009 is equal to the observation. These results indicate a high skill of MME_rcp45 in simulating the observed long-term trend, and the prediction of MME_rcp45 is reasonable. It is expected that the trend of EATs will increase to 1.5±0.37°C by 2040. Its warming rate will be approximately 3°C/100 a during the period 2010–2040.

4 Prediction over 30 years

Re_EATs_int and MME_rcp45 were combined to form the reconstructed decadal component of EATs (Re_EATs) (red dashed line in Figure 5(c)). Compared with EATs (blue solid line in Figure 5(c)), Re_EATs reproduces well the two periods of increase during the 1910s–1930s and 1970s–1990s, and one period of decrease from the mid-1930s to the early-1970s, and has a high correlation coefficient of 0.83. During 2000–2005, Re_EATs shows an upward trend with a warming rate of 0.03°C/a, which qualitatively accords with the trend of EATs (0.007°C/a). The difference of the mean between Re_EATs and the EATs is small (0.02°C). From 2010 to 2040, Re_EATs can be seen to rise during 2010–2015, and decrease thereafter. A cold floor will occur during 2025–2030, and thereafter warm gradually. Because Re_EATs_int decreases continuously from 2030 to 2040, and will be in its negative phase, the warming trend of Re_EATs is a result of anthropogenic forcing. Quantitatively, with a linear trend of 0.01°C/a during 2010–2040, Re_EATs is 1.3±0.64°C by 2040. This result is similar to the prediction from the Hadley Center for the period 2011–2020 (Tollefson, 2013), e.g., the warming phase during 2010–2015, and a slight cooling phase after 2015.

The Re_EATs was compared with the results of the decadal prediction in eight CMIP5 models (Table 2). During 2006–2035 (Figure 6 and Table 4), the linear trends of three models (BCC-CSM1.1, CNRM-CM5, and FGOALS-g2) is negative, while in the remaining five models (CanCM4,

Table 3 Evaluation of the model skill in simulating EATs_trend

Model ID	Correlation coefficient	RMSE (°C)	Model ID	Correlation coefficient	RMSE (°C)
ACCESS1.0	0.79	0.02	GISS-E2-R	0.90	0.01
ACCESS1.3	0.72	0.03	HadGEM2-CC	0.54	0.04
BCC-CSM1.1	0.99	0.01	INM-CM4	0.96	0.01
BCC-CSM1.1(m)	0.99	0.02	IPSL-CM5A-LR	0.99	0.02
CCSM4	0.99	0.001	IPSL-CM5A-MR	0.97	0.01
CESM1-BGC	0.99	0.01	IPSL-CM5B-LR	0.97	0.01
CESM1-CAM5	0.87	0.02	MPI-ESM-LR	0.99	0.02
CSIRO-Mk3.6.0	0.54	0.04	MRI-CGCM3	0.99	0.005
FIO-ESM	0.99	0.01	NorESM1-ME	0.95	0.02
GISS-E2-H	0.97	0.02	MME_rcp45	0.98	0.005

CMCC-CM, IPSL-CM5A, MPI-ESM-LR, and MRI-CGCM3) it is positive, and the MME trend is 0.01°C/a. The mean predicted EATs from the models ranges from 0.3°C to 1.4°C. The MME mean is approximately 0.9±0.3°C. In Figure 6, the EATs in the three models of BCC-CSM1.1, CMCC-CM, and FGOALS-g2 is shown to decrease during 2010–2020, and then increase. The four models of CanCM4, IPSL-CM5A, MPI-ESM-LR, and MRI-CGCM3 show a warming throughout the 30 years, while CNRM-CM5 shows a cooling. The prediction of the MME is stability during 2010–2025, and then a rise. According to the above analyses, the level of uncertainty in the predictions of the models is quite large. Despite the obvious difference between the Re_EATs and modeled curve, the linear trend of Re_EATs (0.002°C/a) is qualitatively in agreement with the trend of most of the models and the MME.

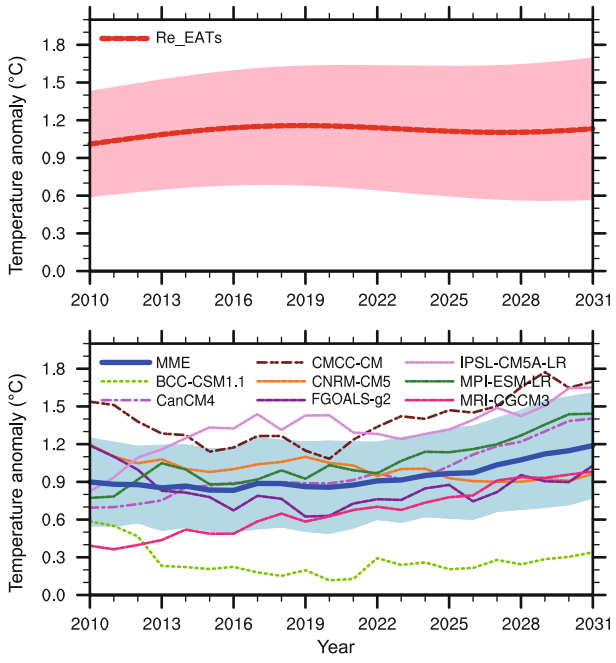

Figure 6 Comparison of Re_EATs with the decadal prediction of CMIP5 models and the MME. Top: temporal evolution of Re_EATs (light red shading indicates the ±1 standard deviation range. Bottom: blue solid line is the temporal evolution of the MME; colored thin lines are the temporal evolutions of the models. The light blue shading indicates the model spread. Unit: °C.

5 Discussion and summary

On the basis of the view that the real climate consists of natural internal variability and external forcing, we predicted EATs over 30 years using a joint statistical-dynamical approach. For the decadal internal variability of EATs (EATs_int), we constructed a multiple linear regression model with predictors of the oceanic modes, considering the lead-lag correlations of the oceanic modes with the EATs_int. The regression model was used to reconstruct EATs_int (Re_EATs_int). It was also applied to obtain the prediction of EATs_int based on the quasi-periods of the decadal oceanic modes. For the anthropogenic forcing, using the output of historical experiments and projections under the RCP4.5 scenario in CMIP5 models, we assessed the historical evolution of EATs via a second fit, and predicted the trend by calculating the MME mean (MME_rcp45). The sum of Re_EATs_int and MME_rcp45 was the reproduced/predicted EATs (Re_EATs). The Re_EATs was compared with the results of the decadal prediction in eight CMIP5 models. The main conclusions can be summarized as follows:

(1) The three oceanic modes (the AMO, IPO and IOBD pattern) account for more than 90% of the internal decadal variance of SST over the North Atlantic, tropical mid-eastern Pacific, Indian Ocean, and tropical western Pacific. The three modes can capture the major features of the decadal internal SST variability.

(2) When EATs_int leads the AMO by 6–7 years, a positive correlation reaches a maximum (correlation coefficient of 0.79). When EATs_int lags the IPO (IOBD pattern) by 10 (5) years, the positive correlation is a maximum, with a correlation coefficient of 0.56 (0.74). The proportions of variance explained by the AMO and IOBD pattern are approximately 30%–40%, whereas the IPO is less than 10%. The total of the proportions is greater than 60% in the Midwest and north, and nearly 30% in the region south of 30°N. Hence, the effects of the oceanic modes can explain most of EATs_int.

(3) Re_EATs_int was reconstructed and predicted by the multiple linear regression model with the three oceanic modes as predictors. During the reconstructed period (1901–1999), Re_EATs_int reproduced the warm and cold

Table 4 Decadal prediction of the Re_EATs and CMIP5 models for 2010–2031

Model ID	BCC-CSM1.1	CanCM4	CMCC-CM	CNRM-CM5	FGOALS-g2
Trend (°C/a)	–0.006	0.03	0.017	–0.01	–0.003
Mean (°C)	0.27	0.1	1.4	1.0	0.84
Model ID	IPSL-CM5A-LR	MPI-ESM-LR	MRI-CGCM3	MME	Re_EATs
Trend (°C/a)	0.025	0.027	0.03	0.01	0.002
Mean (°C)	1.32	1.06	0.66	0.94	1.11

phases in the observation, with a correlation coefficient of 0.7. During the hindcast period (2000–2005), there was little difference between the mean of Re_EATs_int and the observation. The prediction of Re_EATs_int suggested that it would remain stable during 2006–2015, and start to fall after 2015. Furthermore, Re_EATs_int will be in negative phase from 2025 to 2040, which is consistent with the prediction by Qian and Lu (2010).

(4) MME_rcp45 simulated the long-term trend of the observation well during 1901–2009, with a high correlation coefficient of 0.98. The prediction showed MME_rcp45 with a warming rate of 0.3°C/10 a would increase to 1.5±0.37°C by 2040.

(5) During the reconstructed period (1905–1999), Re_EATs corresponded to the upward and downward tendencies in the observation, with a correlation coefficient of 0.83. During the hindcast period (2000–2005), the linear trend of Re_EATs (0.03°C/a) was qualitatively consistent with the observation (0.007°C/a). During the predicted period (2006–2040), Re_EATs was shown to increase during 2010–2015, decrease thereafter until 2030, and then warm again. The Re_EATs, with a linear trend of 0.01°C/yr during the 30 years, was predicted to be 1.3±0.64°C by 2040. Compared with the prediction in the CMIP5 models, the linear trend of Re_EATs is qualitatively in agreement with the trend of most of the models and the MME.

The joint statistical-dynamical approach used in this study for decadal prediction is still at an exploratory stage. Many issues are unclear and deserve further examination. First, the impacts of volcanic eruptions and solar radiation on EATs were not taken into account in the prediction. Compared with decadal hindcast experiments with volcanic eruptions in MPI-ESM-LR, the EATs may be 0.14°C warmer in experiments without volcanic eruptions. The quasi-11-year period of solar radiation was used as a predictor in the regression equation for the model. The regression coefficient of 0.001 indicates that a direct impact of solar radiation does not play a key role. Second, there might be a systematic deviation between the EATs_int obtained by the statistical approach and the MME_rcp45 based on the modeled dataset. We will try to replace EATs_int in future work based on observational records by modeled predictions of EATs. Moreover, no consideration was given to the nonlinear interaction between the internal climate variability and external forcing, which could have great impacts on the prediction. In addition, current knowledge of decadal oceanic modes is insufficient to accurately use the modes for prediction, because of the limitations of the length of instrumental records, the validity of proxy datasets, and the diversity of models (Medhaug and Furevik, 2011). Recent studies (Otterå et al., 2010; Chylek et al., 2010; Wang et al., 2012) have argued that oceanic modes, such as the AMO and PDO, should be influenced by external solar and volcanic forcing. It can be speculated that the evolution of these modes is not regular. Therefore, prediction, based on the quasi-periods of decadal modes, should be noted. Finally, why EATs_int leads the AMO is still unclear in instrumental records. Whether or not it is a real connection in the natural climate system or a result of impacts of the external forcing since the industrial revolution requires further research. In future, as observational data proliferate, climate models improve, and understanding of multi-decadal variability deepens, we will also be able to improve the prediction skill of the joint statistical-dynamical approach.

This study was supported by the National Natural Science Foundation of China (Grant Nos. 41375085, 41421004) and the Strategic Priority Research Program of the Chinese Academy of Sciences (Grant No. XDA05090406).

Allan R J, Lindesay J A, Reason C J C. 1995. Multidecadal variability in the climate system over the Indian Ocean region during the austral summer. J Clim, 8: 1853–1873

Chen W L, Jiang Z H. 2012. Evaluation of the decadal prediction skill over China based on four global atmosphere-ocean coupled climate models (in Chinese). Clim Environ Res, 17: 81–91

Chylek P, Folland C K, Dijkstra H A, et al. 2010. Ice-core data evidence for a prominent near 20 year time-scale of the Atlantic Multidecadal Oscillation. Geophys Res Lett, 38: L13704

Delworth T L, Mann M E. 2000. Observed and simulated multidecadal variability in the Northern Hemisphere. Clim Dyn, 16: 661–671

d'Orgeville M, Peltier W R. 2007. On the Pacific decadal oscillation and the Atlantic multidecadal oscillation: Might they be related? Geophys Res Lett, 34: L23705

Enfield D B, Mestas-Nuñez A M, Trimble P J. 2001. The Atlantic multidecadal oscillation and its relationship to rainfall and river flows in the continental US. Geophys Res Lett, 28: 2077–2080

Folland C K, Parker D E, Colman A W, et al. 1999. Large-scale Modes of Ocean Surface Temperature Since the Late Nineteenth Century. Berlin Heidelberg: Springer. 73–102

Fu C B, Qian C, Wu Z H. 2011. Projection of global mean surface air temperature changes in next 40 years: Uncertainties of climate models and an alternative approach. Sci China Earth Sci, 54: 1400–1406

Gao F, Xin X G, Wu T W. 2012. A study of the prediction of regional and global temperature on decadal time scale with BCC_CSM1.1 Model (in Chinese). Chin J Atmos Sci, 36:1165–1179

Hawkins E, Robson J, Sutton R, et al. 2011. Evaluating the potential for statistical decadal predictions of sea surface temperatures with a perfect model approach. Clim Dyn, 37: 2495–2509

Hoerling M, Hurrell J, Kumar A, et al. 2011. On North American decadal climate for 2011–2020. J Clim, 24: 4519–4528

Hurrell J W, Delworth T L, Danabasoglu G, et al. 2010. Decadal climate prediction: Opportunities and challenges. In: Harrison H J, Stammer D, eds. Proceeding of OceanObs: Sustained Ocean Observations and Information for Society. Venice: ESA Publication

Kaplan A, Cane M A, Kushnir Y, et al. 1998. Analyses of global sea surface temperature 1856–1991. J Geophys Res, 103: 567–589

Keenlyside N S, Latif M, Jungclaus J, et al. 2008. Advancing decadal-scale climate prediction in the North Atlantic sector. Nature, 453: 84–88

Knight J R, Allan R J, Folland C K, et al. 2005. A signature of persistent natural thermohaline circulation cycles in observed climate. Geophys Res Lett, 32: L20708

Li Q, Ren R C, Cai M, et al. 2012. Attribution of the summer warming since 1970s in Indian Ocean Basin to the inter-decadal change in the seasonal timing of El Niño decay phase. Geophys Res Lett, 39: L12702

Li S L, Bates G T. 2007. Influence of the Atlantic Multidecadal Oscillation (AMO) on the winter climate of East China. Adv Atmos Sci, 24: 126–135

Li S L, Luo F F. 2013. Lead-lag connection of the Atlantic Multidecadal

Oscillation (AMO) with East Asian surface air temperatures in instrumental records. Atmos Ocn Sci Lett, 6: 138–143
Luo F F, Li S L, Gao Y Q, et al. 2012. A new method for predicting the decadal component of global SST. Atmos Ocn Sci Lett, 5: 521–526
Medhaug I, Furevik T. 2011. North Atlantic 20th century multidecadal variability in coupled climate models: Sea surface temperature and ocean overturning circulation. Ocean Sci Disc, 8: 353–396
Meehl G A, Goddard L, Murphy J, et al. 2009. Decadal prediction: Can it be skillful? Bull Amer Meteorol Soc, 90: 1467–1485
Mitchell T D, Jones P D. 2005. An improved method of constructing a database of monthly climate observations and associated high resolution grid. Int J Climatol, 25: 693–712
Mochizuki T, Ishii M, Kimoto M, et al. 2010. Pacific decadal oscillation hindcasts relevant to near-term climate prediction. Proc Natl Acad Sci USA, 107: 1833–1837
Murphy J, Kattsov V, Keenlyside N, et al. 2010. Towards prediction of decadal climate variability and change. Proc Environ Sci, 1: 287–304
Otterå O H, Bentsen M, Drange H, et al. 2010. External forcing as a metronome for Atlantic multidecadal variability. Nat Geol, 3: 688–694
Pohlmann H, Johann J H, Köhl A, et al. 2009. Initializing decadal climate predictions with the GECCO oceanic synthesis: Effects on the North Atlantic. J Clim, 22: 3926–3938
Power S, Casey T, Folland C, et al. 1999. Inter-decadal modulation of the impact of ENSO on Australia. Clim Dyn, 15: 319–324
Qian W H, Lu B. 2010. Periodic oscillations in millennial global-mean temperature and their causes. Chin Sci Bull, 55, 4052–4057
Qian W H, Lu B, Zhu C W. 2010. How would global-mean temperature change in the 21st century? Chin Sci Bull, 55: 1963–1967
Rayner N A, Parker D E, Horton E B, et al. 2003. Global analyses of sea surface temperature, sea ice, and night marine air temperature since the late nineteenth century. J Geophys Res, 108: 4407
Smith D M, Cusack S, Colman A W, et al. 2007. Improved surface temperature prediction for the coming decadal from a global climate model. Science, 317: 796–799
Sutton R T, Hodson D L R. 2005. Atlantic Ocean forcing of North American and European summer climate. Science, 309: 115–118
Sutton R T, Hodson D L R. 2007. Climate response to basin-scale warming and cooling of the North Atlantic Ocean. J Clim, 20: 891–907
Tang G L, Ren G Y. 2005. Reanalysis of surface air temperature change of the last 100 years over China (in Chinese). Clim Environ Res, 10: 791–798
Taylor K E, Stouffer R J, Meehl G A. 2012. An overview of CMIP5 and the experiment design. Bull Amer Meteorol Soc, 93: 485–498
Tollefson J. 2013. Climate change: The forecast for 2018 is cloudy with record heat. Nature, 499:139–141
Wang B, Liu M, Yu Y, et al. 2012. Preliminary evaluations of FGOALS_g2 for decadal predictions. Adv Atmos Sci, 30: 674–683
Wang Y M, Li S L, Luo D H. 2009. Seasonal response of Asian monsoonal climate to the Atlantic Multidecadal Oscillation. J Geophys Res, 114: D02112
Wang T, Otterå O H, Gao Y Q, et al. 2012. The response of the North Pacific decadal variability to strong tropical volcanic eruptions. Clim Dyn, 39: 2917–2936
Wu B, Zhou T J. 2012. Prediction of decadal variability of Sea Surface temperature by a coupled global climate model FGOALS_gl developed in LASG/IAP. Chin Sci Bull, 57: 2453–2459